RSC Advances

PAPER

View Article Online
View Journal | View Issue

Cite this: *RSC Adv.*, 2023, **13**, 16165

Experimental investigation of nanofluid enhanced oil recovery by spontaneous imbibition

Jingnan Zhang, *[ab] Hai Huang,[b] Ming Zhang[b] and Wenchang Wang*[c]

Nanofluids have been recently proposed as new chemical agents for enhanced oil recovery. In this study, in order to reflect the effect of nanofluids on imbibition, the imbibition performance of manganese chloride ($MnCl_2$) solution, sodium dodecylbenzene sulfonate (SDBS) solution, and silica (SiO_2) nanofluids were studied by a spontaneous imbibition experiment at 25 °C and 0 MPa. The oil production from pores with different sizes and the imbibition efficiency were tested by nuclear magnetic resonance T_2 spectroscopy and metering in spontaneous imbibition. In addition, the interfacial tensions between the imbibition liquids and oil were tested. The changes in the contact angle of the core slice before and after immersing in imbibition liquids were measured. The silica nanofluid is used as the imbibition liquid, and the shift of the T_2 spectral peak to the left is not obvious and shifted by only 23.95–25.72 ms, the change in the contact angle is 6.63°–12°, the interfacial tension between the nanofluid and the simulated oil is 0.25–0.41 mN m^{-1}, and the imbibition efficiency was slightly improved with increasing nanoparticle concentration, up to 57.40%, which improved by 16.14% and 32.95%, respectively, compared to the surfactant solution and the manganese chloride solution. This shows that the silica nanofluid can effectively improve oil production in small pores, reduce oil–water interfacial tension, and change rock wettability.

Received 26th October 2022
Accepted 13th May 2023

DOI: 10.1039/d2ra06762e

rsc.li/rsc-advances

Introduction

Low oil recovery has always been the bottleneck in oilfield development. With the increasing advancement and diversification of research methods, scholars have made some progress in studying nanofluid enhanced oil recovery (EOR). The nanofluid flooding oil experiments were conducted with macro homogeneous and heterogeneous cores, and they had a better effect on experiments.[1–5] Some experiments show that the nanofluids can enter the rock pore network, change the surface properties of the pore wall, strengthen the attraction between the particles and the pore wall, and effectively increase the oil displacement efficiency.[6,7] Moradi *et al.*[8] conducted core displacement experiments by alternating the injection of nanofluids and carbon dioxide gas. It was found that the recovery efficiency of nanofluids was higher than that of regular alternating injection of gas and water. The displacement effect was better in a low permeability core (2.839 mD), and the smaller the nanoparticles, the better the displacement effect. Lei *et al.*[9] tested the effect of nanofluids on expanding the swept volume of an ultralow-permeability core in a core flooding experiment. The experimental results show that nanofluids can weaken the hydrogen bond association between water molecules and effectively change the structure of the water molecular network. Thus, nanofluids enter the small, low-permeability pore area that cannot be swept by conventional water flooding. Jafarbeigi *et al.*[10] evaluated the oil displacement effect of nanofluids on the carbonate reservoir through a core displacement experiment. The results show that the nanofluids can effectively change the wettability of the rock surface in the carbonate reservoir, and the recovery after displacement can increase by 15–23%. Liu *et al.*[11] added Janus-silica nanoparticles to the surfactant and recovery was significantly improved under the same displacement condition, showing good EOR potential. Jalilian *et al.*[12] investigated the feasibility of nano-emulsion flooding as a method for EOR through core flooding experiments and a recovery factor of up to 60%.

The above experiments show that nanofluids have an excellent oil displacement effect. Spontaneous imbibition is a process in a porous medium that spontaneously absorbs a wetting liquid driven by capillary force, which plays a vital role in EOR.[13] Due to the gradual transition of oil production from a simple homogeneous reservoir to a fractured dual-porosity reservoir,[14] spontaneous imbibition has attracted extensive attention from scholars. The spontaneous imbibition experiments were conducted using water or surfactant solutions.[15–20] Standnes *et al.*[21] conducted spontaneous imbibition experiments using aqueous solutions of ethoxylated alcohol (EA) and

[a]*School of Urban Planning and Municipal Engineering, Xi'an Polytechnic University, China*

[b]*Shaanxi Key Laboratory of Advanced Stimulation Technology for Oil & Gas Reservoirs, Xi'an Shiyou University, China*

[c]*School of Mechanics and Engineering Science, Shanghai Institute of Applied Mathematics and Mechanics, Shanghai University, China*

a cationic surfactant (C12TAB). For the short core experiments, about 40–45% of the original oil in place (OOIP) was recovered using C12TAB, while only 10% was the average recovery using EA. Contact angle measurements on oil-wet calcite crystals confirmed that C12TAB was much more effective than EA in altering wettability in water-wet conditions. Habibi *et al.*[22] performed different sets of experiments to investigate surfactants with long and short ethoxylate (EO) chains that enhance imbibition. These experiments show that the wettability alteration is the primary mechanism of the surfactant solution to improve the imbibition efficiency. However, many types of research have shown that nanofluid can effectively change the wettability of the rock.[23–28] Caili Dai *et al.*[29] prepared a new kind of self-dispersing silica nanoparticle and used it to enhance oil recovery in spontaneous imbibition experiments of low-permeability cores. The excellent performance of nanofluids was attributed to the fact that nanofluids could significantly change the wettability of rocks. Moghaddam *et al.*[30] investigated the impacts of the nanofluids of zirconium dioxide, calcium carbonate, titanium dioxide, silicon dioxide, magnesium oxide, aluminium oxide, cerium oxide, and carbon nanotube on the wettability of carbonate rocks by spontaneous imbibition. The results of spontaneous imbibition tests confirm the active roles of calcium carbonate and silicon dioxide nanoparticles in EOR.

In this study, a method of spontaneous imbibition experiment was adopted. Manganese chloride solution, sodium dodecylbenzene sulfonate solution, and silica nanofluid with different concentrations were used to enhance oil recovery in spontaneous imbibition. Significantly, the imbibition efficiency of different imbibition liquids in the spontaneous imbibition process was measured by metering and nuclear magnetic resonance T_2 spectrum, avoiding the inaccuracy caused by using a single metering method. In addition, the interfacial tensions between different imbibition liquids and oil were tested. The change in the contact angle of the core slices before and after immersing in different imbibition liquids was measured. Furthermore, the mechanism of nanofluids in enhanced oil recovery by spontaneous imbibition was analysed.

Imbibition experiment

Experimental materials

Imbibition liquid 1#. Deionized water with manganese chloride of 0.5 wt%. The purpose of using manganese chloride is to test the NMR T_2 spectrum. The experiments show that a 0.5 wt% manganese chloride aqueous solution instead of water can distinguish the NMR signals of oil and water.[31] Manganese chloride was purchased from Sinopharm Chemical Reagent Co. Ltd., with a purity of 99.9 wt%.

Imbibition liquid 2#. Surfactant solution consisting mainly 0.5 wt% of sodium dodecylbenzene sulfonate and 0.5 wt% of manganese chloride. Sodium dodecylbenzene sulfonate was purchased from Sinopharm Chemical Reagent Co. Ltd., with a purity of 99.0 wt%.

Imbibition liquid 3#. Nanofluid mainly composed of silica nanoparticles (0.5 wt%), sodium dodecylbenzene sulfonate (0.5 wt%), and manganese chloride (0.5 wt%). Silica nanoparticles were prepared in the laboratory with an average particle size of 20 nm and purity of over 99.8%.

Imbibition liquid 4#. Nanofluid mainly composed of silica nanoparticles (1.0 wt%), sodium dodecylbenzene sulfonate (0.5 wt%), and manganese chloride (0.5 wt%). Silica nanoparticles were prepared in the laboratory with an average particle size of 20 nm and purity of over 99.8%.

Imbibition liquid 5#. Nanofluid mainly composed of silica nanoparticles (1.5 wt%), sodium dodecylbenzene sulfonate (0.5 wt%), and manganese chloride (0.5 wt%). Silica nanoparticles were prepared in the laboratory with an average particle size of 20 nm and purity of over 99.8%.

Imbibition liquid 6#. Nanofluid mainly composed of silica nanoparticles (2.0 wt%), sodium dodecylbenzene sulfonate (0.5 wt%), and manganese chloride (0.5 wt%). Silica nanoparticles were prepared in the laboratory with an average particle size of 20 nm and purity of over 99.8%. The preparation methods of the imbibition liquid 1#–6# include: ① the nanoparticles were added into deionized water and stirred with the magnetic force for 10 min at 25 °C. ② The manganese chloride was added to the liquid prepared in the previous step and continued to stir with the magnetic force for 10 min at 25 °C. ③ The SDBS was added to the liquid prepared in the previous step and stirred again for 10 min with magnetic force at 25 °C. ④ The liquid prepared in the previous step was subjected to ultrasonic vibration for 30 min at 25 °C and 40 kHz.

Simulated oil. Filtered diesel oil and crude oil were prepared according to the mass ratio of 10 : 1, and the viscosity was 2.5 mPa s at 25 °C.

Cores. The experimental cores are artificial homogeneous sandstone, and the pre-treatment methods include: ① the magnetism of the cores was detected and prevented interference with the magnetic field. ② The physical parameters of the core were tested. ③ The cores were cut into core sections with a length of about 3 cm and core slices with a thickness of about 0.3 cm, the core sections were numbered c-3-2-1, c-3-2-2, c-3-2-3, c-3-3-1, c-3-3-2, c-3-3-3 and the core slices were numbered s-3-2-1, s-3-2-2, s-3-2-3, s-3-3-1, s-3-3-2, s-3-3-3, respectively. ④ The core sections and core slices were placed in an oven and dried at 80 °C for 24 h after washing the surface residue. ⑤ The length of each core section and the core slice was measured, and the mass (dry weight) of the core sections was weighed. ⑥ The core sections were put in the vacuum pressurized saturation device and saturated with an aqueous manganese chloride solution. ⑦ The core sections were removed to weigh the wet weight and measure the pore volume (PV). ⑧ The bound water of the core sections was established by oil flooding manganese chloride aqueous solution in a flooding device. The volume of the injected oil was recorded when the water content at the outlet of the section was 0. ⑨ Closing all valves of the flooding device and making the oil was aged for 48 h in core sections. It is worth noting that the 0.5 wt% manganese chloride aqueous solution was used in the above steps. The physical parameters of the core sections and core slices are shown in Table 1.

Table 1 Physical parameters of core sections and core slices

Number	Length/cm	Diameter/cm	Porosity/%	Permeability/10^{-3} μm^2	S_{oi}/%	S_{wi}/%	Remarks	Rock type
3-2	10.00	2.52	32.25	1012.20	—	—	Core	Sandstone
3-3	10.00	2.52	28.65	987.36	—	—	Core	Sandstone
c-3-2-1	2.92	2.52	31.67	—	72.78	27.22	Core section	Sandstone
c-3-2-2	2.88	2.52	32.05	—	76.32	23.68	Core section	Sandstone
c-3-2-3	2.86	2.52	31.52	—	78.06	21.94	Core section	Sandstone
c-3-3-1	2.78	2.52	30.28	—	69.52	30.48	Core section	Sandstone
c-3-3-2	2.96	2.52	26.32	—	66.36	33.64	Core section	Sandstone
c-3-3-3	2.62	2.52	27.66	—	67.22	32.78	Core section	Sandstone
s-3-2-1	0.28	2.52	—	—	—	—	Core slice	Sandstone
s-3-2-2	0.28	2.52	—	—	—	—	Core slice	Sandstone
s-3-2-3	0.26	2.52	—	—	—	—	Core slice	Sandstone
s-3-3-1	0.26	2.52	—	—	—	—	Core slice	Sandstone
s-3-3-2	0.24	2.52	—	—	—	—	Core slice	Sandstone
s-3-3-3	0.27	2.52	—	—	—	—	Core slice	Sandstone

Experimental equipment and methods

Spontaneous imbibition experiment. The experimental device for core spontaneous imbibition is shown in Fig. 1. The upper part is a metering tube with a scale, which can read the volume of discharged oil, *i.e.*, the metering method. A circular cavity below the metering tube, which is connected to the bottle, can be separated so that the core can be put into it. A water outlet is arranged below the bottle. The core support is set at the bottom of the bottle to avoid large-area contact between the surface beneath the core and the bottom of the bottle, preventing the imbibition efficiency from being affected.

The experimental steps are as follows:

(1) The saturated oil core sections were tested with nuclear magnetic resonance. The experimental devices for spontaneous imbibition were numbered 1#, 2#, 3#, 4#, 5#, and 6#, then the core section c-3-2-1, c-3-2-2, c-3-2-3, c-3-3-1, c-3-3-2, and c-3-3-3 were placed in device 1#, device 2#, device 3#, device 4#, device 5#, and device 6#, respectively. Apply Vaseline evenly to the contact surface between the glass cavity and the bottle, and then closely connect the glass cavity and the bottle.

(2) The prepared imbibition liquid 1#, imbibition liquid 2#, imbibition liquid 3#, imbibition liquid 4#, imbibition liquid 5#, and imbibition liquid 6#, were slowly poured from the top of the metering tube into device 1#, device 2#, and device 3#, device 4#, device 5#, and device 6#, respectively.

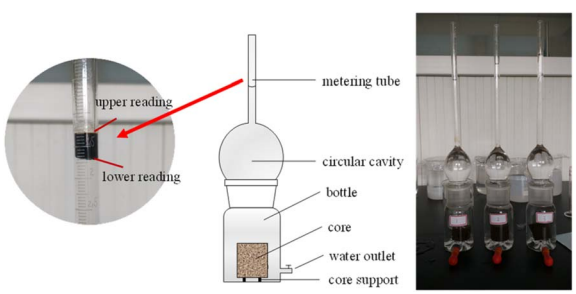

Fig. 1 The experimental device for core spontaneous imbibition.

(3) Upper and lower readings in the metering tube were recorded every 2 h.

(4) The oil in the tube was sucked out from the top of the metering tube, and the rest of the liquids were drained slowly through the discharge when there was no change in the difference between the upper reading and the lower reading of the metering tube for 10 h. The cores were removed, drained, and wrapped with polyethylene film for use in the next step.

The imbibition efficiency is obtained from the following:

$$E_m = \frac{V_{upper} - V_{lower}}{V_{oil}} \times 100\% \quad (1)$$

where E_m is the imbibition efficiency measured by metering; V_{upper} is the upper reading of the metering tube, mL; V_{lower} is the lower reading of the metering tube, mL; V_{oil} is the saturated oil volume of the core, mL.

Nuclear magnetic resonance test. Nuclear magnetic resonance (NMR) equipment mainly includes industrial computers, spectrometer systems, radio frequency systems (RF), gradient systems, magnet cabinets, *etc.* The performance parameters of the equipment are shown in Table 2.

The core was placed in the NMR equipment RF coil to test its T_2 spectrum when the core was saturated with oil at the end of imbibition. The schematic diagram of the T_2 spectrum is shown in Fig. 2.

The peak area (cumulative signal amplitude in shaded area) in the relaxation curve is directly proportional to the liquid quality in the core, and the T_2 value at the peak point is proportional to the size of the pore where the liquid in the core is located. Therefore, the degree of oil production in pores of different sizes can be reflected by the NMR T_2 spectrum.[18]

Interfacial tension measurement. The JJ2000B rotary drop interfacial tension measuring instrument is used, which mainly includes a high-speed motor, sample tank, lens barrel, and charge coupled device (CCD) camera. The main technical parameters are shown in Table 3.

The interfacial tensions between the imbibition liquid and the simulated oil were measured by the pendant drop method. During the measurement, the simulated oil and imbibition

Table 2 The performance parameters of the equipment

Performance	Parameters
Magnet type	Permanent magnet
Magnetic field intensity	(0.50 ± 0.05) T
Magnetic field stability	≤300 Hz h^{-1}
RF field	Pulse frequency 1–30 MHz, frequency control accuracy 0.1 Hz, pulse accuracy 100 ns
RF transmission power	Peak output > 300 W
Maximum sampling bandwidth	2000 kHz
Imaging gradient	Peak intensity > 2.5 G cm^{-1}
Probe coil diameter	60 mm
Effective sample detection range	60 mm diameter sphere
Imaging quality	The image signal-to-noise ratio is greater than 20 dB, the image distortion is less than 15%, and the image uniformity is greater than 45%
Sampling frequency	50 MHz

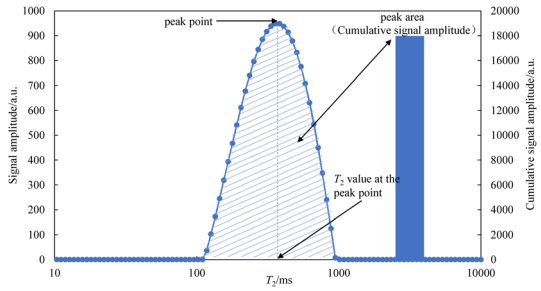

Fig. 2 Schematic diagram of the T_2 spectrum.

liquids were added to the sample tube to form the interface. The sample tube rotation speed was set at 2000 rpm, and the temperature was set at 25 °C. Under centrifugal force, gravity, and interfacial tension, the lighter liquid forms a long ellipsoid or cylindrical droplet in the heavier liquid. Under the horizontal condition of the rotation axis, the droplet length of $2x_0$ and width of $2y_0$, and the interfacial tension are calculated according to the Bashforth–Adams equation:

$$\gamma = \frac{1}{4}\Delta\rho\omega^2 {y_0}^3 f \quad (2)$$

where γ is the interfacial tension, mN m; $\Delta\rho$ is the density difference between the liquid–liquid phase or the gas–liquid phase, g mL; ω is the angular velocity of the system rotation, rpm; y_0 is half of the droplet width, cm; f is the correction factor, determined by x_0/y_0.

Contact angle measurement. The core slices were cleaned and put in the vacuum oven for 24 h. Then, soaked in deionized water for 24 h, the contact angle of the core slices was tested according to the method shown in Fig. 3 using the OCA20 video contact angle measuring instrument. After that, the core slices were put into the vacuum oven again for 24 h. After taking them out, the core slice s-3-2-1, core slice s-3-2-2, core slice s-3-2-3, core slice s-3-3-1, core slice s-3-3-2, core slice s-3-3-3 were immersed separately in imbibition liquid 1#, imbibition liquid 2#, imbibition liquid 3#, imbibition liquid 4#, imbibition liquid 5#, imbibition liquid 6#, and immersed for 24 h. The contact angle was tested again after the core slices were removed. It is noteworthy that three different positions of each core slice were tested, and the average value of the contact angle was obtained from different positions as the test result.

Overall experimental procedure. The general experimental procedure is shown in Fig. 4.

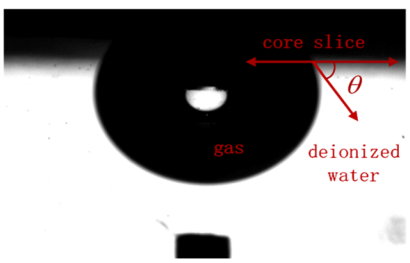

Fig. 3 Schematic diagram of the contact angle test.

Table 3 The main parameters of JJ2000B rotating drop interfacial tension measuring instrument

Performance	Parameters
Tension measurement range	10^{-6}–500 mN m^{-1}
Rotating shaft speed	1000 rpm–20 000 rpm
Speed accuracy	1‰
The inner diameter of the capillary tube for measurement	4 mm/2 mm
Light source	70 × 19 mm plane tube 12 V
T-Head for two kinds of amplification factor measurement	2 mm/1.1 mm

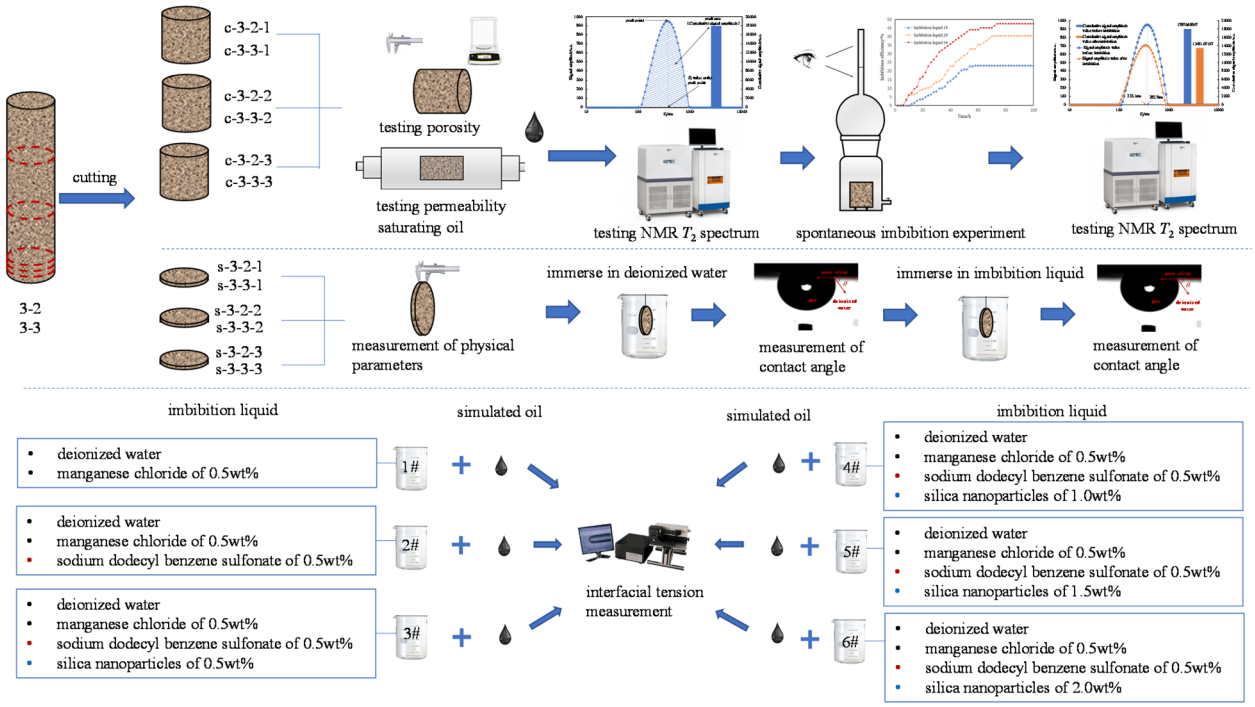

Fig. 4 Overall experimental procedure.

Experimental results and discussion

Imbibition efficiency

The imbibition efficiency of the core in three kinds of imbibition liquids was studied using metering and T_2 spectrum testing. The metering method is the most convenient and intuitive, and it can be obtained directly by reading the scale of the metering tube of the imbibition device. The curve of imbibition efficiency with time obtained by the metering method at 25 °C is shown in Fig. 5.

The final imbibition efficiency of imbibition liquid 1#, imbibition liquid 2#, imbibition liquid 3#, imbibition liquid 4#, imbibition liquid 5#, and imbibition liquid 6# is 23.20%, 40.50%, 47.54%, 52.22%, 55.06%, and 55.87%, respectively. It can be seen from the figure that the oil in the imbibition liquid 3#–6# is discharged relatively quickly. This shows that the imbibition liquid 3#–6# has a better performance in imbibition and oil drainage compared to other imbibition liquids.

Before saturating the rock with oil, the T_2 spectrum of the oil as a bulk is shown in Fig. 6.

As can be seen from Fig. 6, when a large oil droplet exists in the sample bottle, the position of its peak vertex is 666.99 ms, and the peak area is 27 783.96 a.u.

The T_2 spectrum of oily cores before and after spontaneous imbibition in three kinds of imbibition liquids is shown in Fig. 7–12. It is worth noting that the core used in this experiment is an artificial sandstone core. If repeated cleaning is performed, the permeability and porosity of the core will be affected, resulting in the differences in the physical parameters of the same sample at different experimental stages. Therefore, two cores (about 10 cm in length) of the same batch with similar physical parameters are selected, and in this study, six core sections (about 3 cm in length) formed after cutting are not reused.

As can be seen in Fig. 7–12, the peak point of the spectrum shifted to the left during imbibition. The peak point of the T_2

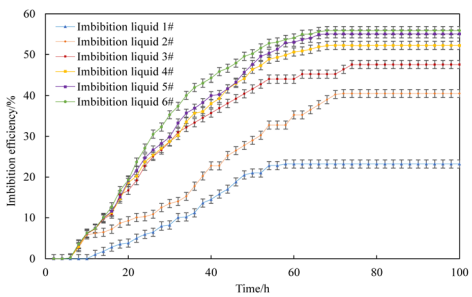

Fig. 5 The curve of imbibition efficiency with time (25 °C).

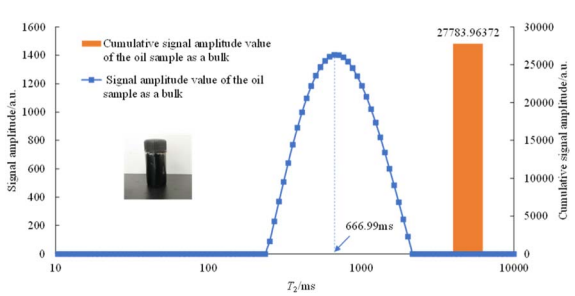

Fig. 6 The T_2 spectrum of the oil sample as a bulk.

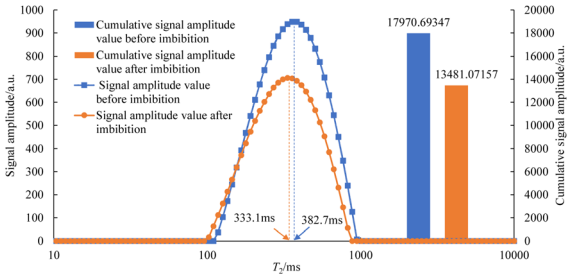

Fig. 7 T_2 spectrum of the core c-3-2-1 before and after imbibition.

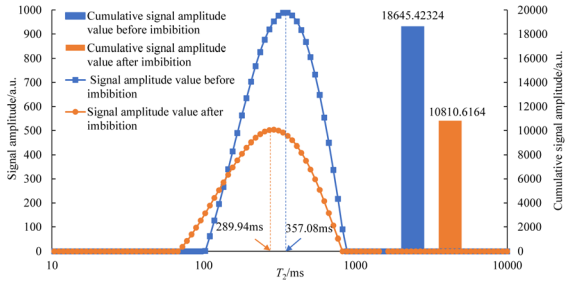

Fig. 8 T_2 spectrum of the core c-3-2-2 before and after imbibition.

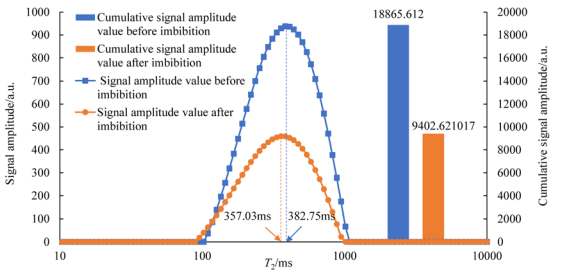

Fig. 9 T_2 spectrum of the core c-3-2-3 before and after imbibition.

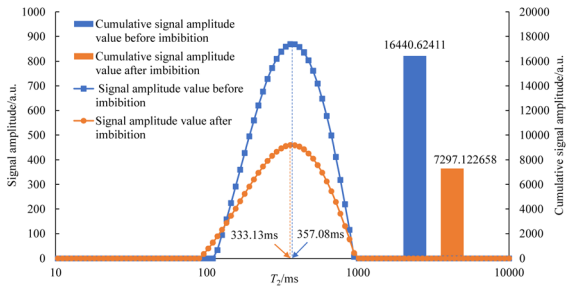

Fig. 10 T_2 spectrum of the core c-3-3-1 before and after imbibition.

spectrum for the core c-3-2-2 in imbibition liquid 2# moved to the left obviously during imbibition by 67.14 ms. The peak point of the T_2 spectrum for the core c-3-2-3, c-3-3-1, c-3-3-2, and c-3-3-3 in imbibition liquid 3#–6# moving to the left is not obvious during imbibition and shifts by only 23.95–25.67 ms. It shows that the oil in relatively large pores is highly produced under the action of imbibition liquid 2#. The degree of oil production in

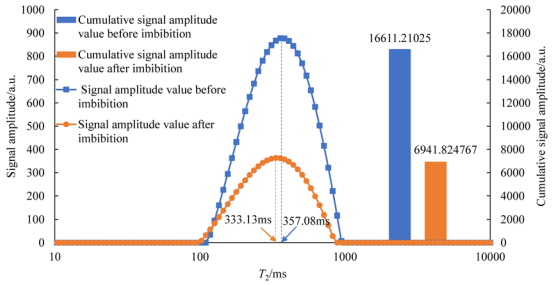

Fig. 11 T_2 spectrum of the core c-3-3-2 before and after imbibition.

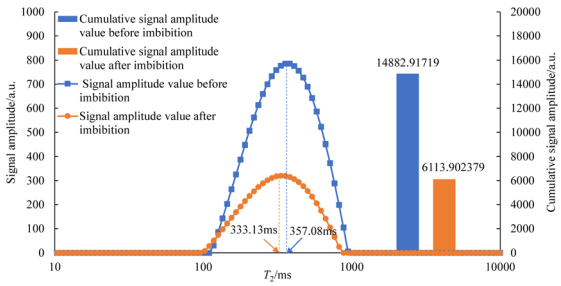

Fig. 12 T_2 spectrum of the core c-3-3-3 before and after imbibition.

the core pores under the action of the imbibition liquid 3#–6# is relatively uniform. It also suggests that imbibition liquid 3# can increase the degree of oil production in small pores compared to imbibition liquid 1# and imbibition liquid 2#.

After imbibition, the peak area (the cumulative signal amplitude in the area enclosed by the T_2 curve and abscissa) of core c-3-2-1, c-3-2-2, c-3-2-3, c-3-3-1, c-3-3-2, c-3-3-3 decreased by 4489.62, 7834.81, 9462.99, 9152.50, 9669.39, 8769.02 a.u., respectively. The peak area is proportional to the oil saturation, so the decrease in the peak area is the imbibition efficiency of the core in the imbibition process, which can be calculated using the following:

$$E_n = \frac{A_{oi} - A_o}{A_{oi}} \times 100\% \quad (3)$$

where E_n is the imbibition efficiency measured by nuclear magnetic resonance; A_{oi} is the peak area (a.u.) of the core before imbibition; A_o is the peak area (a.u.) of the core after imbibition.

The imbibition efficiency obtained by the T_2 spectrum is shown in Table 4. This indicates that core 3# has the highest imbibition efficiency, which is close to the results obtained by metering. But there are still some differences. This is because the volume of oil floating on the upper surface due to gravity differentiation in the imbibition process was measured by metering, and a small amount of oil dissolved in the imbibition liquid or attached to the vessel was not considered. When the reduction of oil in the core was tested by using the nuclear magnetic resonance T_2 spectrum method, the residual oil in the core would run off in the process of core extraction, which will be mistaken for the result of imbibition. Thus, it can be seen that the use of the metering method will get a smaller result

Table 4 The average of the imbibition efficiency

Imbibition liquid number	Imbibition efficiency		
	Metering	T_2 spectrum	Average value
1#	23.20%	24.98%	24.09%
2#	40.50%	42.02%	41.26%
3#	47.54%	50.16%	48.85%
4#	52.22%	55.67%	53.95%
5#	55.06%	58.21%	56.64%
6#	55.87%	58.92%	57.40%

than the actual value, while the use of the nuclear magnetic resonance T_2 spectrum method will get a larger result than the actual value. So, we need to take the average of the two results in order to obtain more accurate results. The average of the imbibition efficiency is also shown in Table 4.

The relationship between fluid composition and imbibition efficiency is shown in Fig. 13.

It can be seen from Fig. 13 that with the increase in composition, the imbibition efficiency is significantly improved. After the composition of nanoparticles is added, the imbibition efficiency is further improved, which shows that the nanofluid used in this study effectively improves the imbibition efficiency. With increasing nanoparticle concentration, the imbibition efficiency was slightly improved.

Interfacial tension between imbibition liquids and oil

The interfacial tension between imbibition liquids and oil is shown in Table 5.

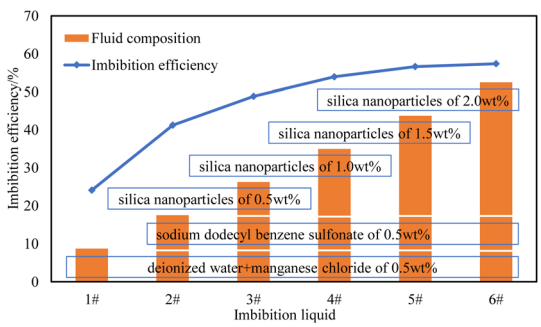

Fig. 13 Relationship between fluid composition and imbibition efficiency.

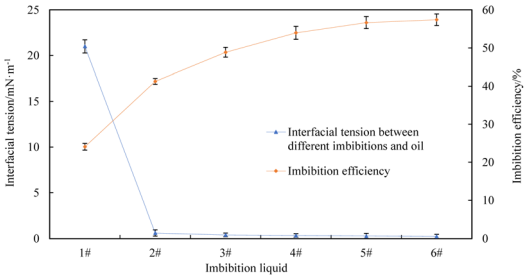

Fig. 14 Relationship between interfacial tension and imbibition efficiency.

The interfacial tensions between imbibition liquid 2#–6# and oil are significantly reduced compared to the interfacial tension between imbibition liquid 1# and oil because imbibition liquid 3# and imbibition liquid 2# contain the same surfactant composition, which can reduce the oil–water interfacial tension. The interfacial tension between imbibition liquid 3#–6# and oil is closer to that between imbibition liquid 2# and oil. It shows that the composition of the nanoparticle in the imbibition liquid 3#–6# does not have a noticeable effect on reducing the oil–water interfacial tension. The imbibition efficiency and the corresponding interfacial tension values are shown in Fig. 14.

The interfacial tensions of imbibition liquid 2#–6# and oil were significantly lower than those of imbibition liquid 1# and oil, and the imbibition efficiencies of imbibition liquid 2#–6# are also significantly higher than that of imbibition liquid 1#, which indicates that the reduction of the oil–water interfacial tension is one of the main factors to improve the imbibition efficiency in the spontaneous imbibition process. The oil in the core deforms more easily as the oil–water interfacial tension decreases. The ability of oil droplets to pass through the throat of a porous medium will be enhanced. A part of the immovable oil is changed into movable oil and discharged from the core by the action of imbibition. Thus, imbibition efficiency is improved effectively.

The contact angle of core slices

The liquid–solid contact angles of the core slice s-3-2-1, s-3-2-2, s-3-2-3, s-3-3-1, s-3-3-2, and s-3-3-3 immersed in imbibition liquids for 24 h are shown in Table 6.

The core slices show water-wet characteristics after immersing in deionized water for 24 h. The contact angles of

Table 5 The interfacial tension between imbibition liquids and simulated oil

Imbibition liquid	Test 1 interfacial tension/(mN m^{-1})	Test 2 interfacial tension/(mN m^{-1})	Test 3 interfacial tension/(mN m^{-1})	Average interfacial tension/(mN m^{-1})
1#	21.01	21.24	20.75	21.00
2#	0.89	0.46	0.51	0.62
3#	0.43	0.55	0.25	0.41
4#	0.52	0.28	0.36	0.35
5#	0.48	0.16	0.22	0.29
6#	0.27	0.31	0.18	0.25

Table 6 The liquid–solid contact angles of the core slices

Core slices	Condition	Test 1 liquid–solid contact angles/°	Test 2 liquid–solid contact angles/°	Test 3 liquid–solid contact angles/°	Average liquid–solid contact angles/°	The change of contact angle/°
s-3-2-1	Immerse in deionized water for 24 h	66.51	64.25	66.43	65.73	0.68
	Immerse in imbibition liquid 1# for 24 h	66.25	67.43	65.55	66.40	
s-3-2-2	Immerse in deionized water for 24 h	64.76	62.85	63.49	63.70	4.27
	Immerse in imbibition liquid 2# for 24 h	68.42	67.13	68.36	67.97	
s-3-2-3	Immerse in deionized water for 24 h	65.12	65.26	67.32	65.90	6.63
	Immerse in imbibition liquid 3# for 24 h	72.63	71.78	73.18	72.53	
s-3-3-1	Immerse in deionized water for 24 h	64.68	65.81	62.27	64.25	8.81
	Immerse in imbibition liquid 4# for 24 h	71.68	72.28	75.21	73.06	
s-3-3-2	Immerse in deionized water for 24 h	64.92	66.32	67.62	66.3	10.98
	Immerse in imbibition liquid 5# for 24 h	75.38	76.92	79.55	77.28	
s-3-3-3	Immerse in deionized water for 24 h	63.21	63.31	65.52	64.01	12
	Immerse in imbibition liquid 6# for 24 h	77.82	75.98	74.22	76.01	

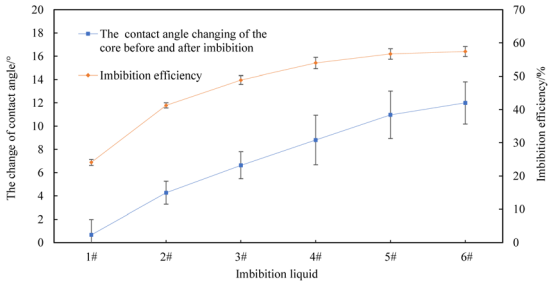

Fig. 15 Relationships between the change value of the contact angle and the imbibition efficiency.

the core slice after immersing in imbibition liquid 2#–6# have increased compared to those after immersing in deionized water, which indicates that the wettability of the core surface can be changed by imbibition liquid 2#–6#. The relationships between the change value of the contact angle and the imbibition efficiency of the core slices before and after immersion in different imbibition liquids are shown in Fig. 15.

The higher the value of contact angle change before and after the core slices are immersed in different imbibition liquids, the higher the imbibition efficiency, indicating that the change in rock wettability is one of the factors in improving the imbibition efficiency in the process of spontaneous imbibition. In addition, it can be seen from Fig. 14 and 15 that the interfacial tension between oil and imbibition liquid 2#–6# are relatively close. The wettability changes of the core slice immersed in liquid 2#–6# are also not obvious. But the imbibition efficiency of the core section in imbibition liquid 2# is lower than that of imbibition liquid 3#–6#. This is because the imbibition liquid 3#–6# contains nanoparticles. Wasan and Nikolov *et al.* found that the nanoparticles were arranged spontaneously and orderly in the three-phase contact wedge region, which generated structural disjoining pressure. The nanofluid film continuously diffused to the centre of the contact region between oil droplets and the solid phase surface under the action of structural disjoining pressure. Finally, the oil droplets were driven away.[32–34] Zhang Hua *et al.*[35] performed a series of flooding experiments on EOR using a nanofluid at different capillary numbers. Additional oil recovery of around 15% may be achieved by a nanofluid compared to brine at a Ca $= 10^{-7}$ insufficient time for the nanofluid film to advance through structural disjoining pressure and displace oil. Compared to oil recovery by the SDS solution and the nanofluid with the same IFT, the additional oil by the nanofluid is 12.6% and is also due to the structural disjoining pressure. Dai Caili *et al.*[29] measured the contact angle and interfacial tension to investigate the mechanism of nanoparticles for enhanced oil recovery. The results showed that the adsorption of silica nanoparticles can change the surface wettability from oil-wet to water-wet and silica nanoparticles showed little influence on oil/water interfacial tension. In addition, the change of the oil droplet shape on the hydrophobic surface was monitored through dynamic contact angle measurement. It was shown that silica nanoparticles can gradually detach the oil droplet from the hydrophobic surface,

which is consistent with the structural disjoining pressure mechanism proposed by Wasan and Nikolov. Similarly, the nanofluids used in this experiment have no significant effect on the wettability of sandstone core slices and the interfacial tension between oil and water. However, the imbibition efficiency was increased using nanofluids in comparison to that of saline and surfactant solutions. This is also consistent with the structural disjoining pressure mechanism. Therefore, the reduction of the interfacial tension and the change in rock wettability are the two significant factors in improving the imbibition efficiency of the surfactant solution and the nanofluid. At the same time, nanofluids have a strong ability to peel oil droplets and achieve a better imbibition effect due to the structural disjoining pressure.

This study shows that nanofluids have good performance and great potential to improve imbibition efficiency. Overall, the contact angle is around 70, indicating water-wet conditions, and the reduction in IFT is not high, which indicates poor chemical performance. Oil-wet samples such as carbonate are worth studying. The factors influencing the imbibition efficiency and the optimal formula of nanofluids need to be further studied in order to promote the improvement, popularization, and industrial application of nanofluids for EOR.

Conclusions

The manganese chloride solution, sodium dodecylbenzene sulfonate solution, and silica nanofluid were used to investigate their performance for imbibition. The imbibition efficiency was the best and reached 57.40% when the core was immersed in 2.0 wt% silica nanofluid under the conditions used in this paper. With increasing nanoparticle concentration, the imbibition efficiency was slightly improved. The NMR T_2 spectrum showed that the degree of oil production in the small pores of the core was increased in the imbibition process with a silica nanofluid. During imbibition, the interfacial tension between oil and water can be reduced, and the wettability of the rock can be changed by sodium dodecylbenzene sulfonate solution and silica nanofluid, which are two dominant factors in improving the efficiency of core imbibition. In addition, silica nanofluid has a strong ability to peel off oil droplets due to the structural disjoining pressure, which can achieve better imbibition efficiency compared to sodium dodecylbenzene sulfonate solution (no silica particles). We hope that this work can be helpful to the applications of nanofluids for EOR.

Author contributions

Jingnan Zhang: conceptualization, data curation, formal analysis, and writing – original draft; Wenchang Wang: data curation, methodology, writing – review & editing; Hai Huang: formal analysis, funding acquisition; Ming Zhang: methodology, investigation.

Conflicts of interest

There are no conflicts to declare.

Acknowledgements

This research is supported by the Open Fund Project of the Shaanxi Key Laboratory of Advanced Stimulation Technology for Oil & Gas Reservoirs (kfjj-tz-2020-5), Initial Scientific Research Fund of Doctoral in Xi'an Polytechnic University (201933), National Natural Science Foundation of China (51874240), Natural Science Basic Research Program of Shaanxi (2022-JQ-057), Key Research and Development Program of Shaanxi (2020kw-027), Natural Science Basic Research Program of Shaanxi (2023-JC-QN-0400).

Notes and references

1 B. Suleimanov, F. Ismailov and E. Veliyev, *J. Pet. Sci. Eng.*, 2011, **78**, 431–437.
2 Z. Hu, S. M. Azmi, G. Raza, P. W. Glover and D. Wen, *Energy Fuels*, 2016, **30**, 2791–2804.
3 M. Zargartalebi, R. Kharrat and N. Barati, *Fuel*, 2015, **143**, 21–27.
4 H. Ehtesabi, M. M. Ahadian, V. Taghikhani and M. H. Ghazanfari, *Energy Fuels*, 2014, **28**, 423–430.
5 H. Ehtesabi, M. M. Ahadian and V. Taghikhani, *Energy Fuels*, 2015, **29**, 1–8.
6 L. Hendraningrat, S. Li and O. Torsæter, *J. Pet. Sci. Eng.*, 2013, **111**, 128–138.
7 H. Reza, P. Peyman, V. Ali and S. Abdolhamid, *Pet. Explor. Dev.*, 2017, **44**, 802–810.
8 B. Moradi, P. Pourafshary, F. Jalali, M. Mohammadi and M. Emadi, *J. Nat. Gas Sci. Eng.*, 2015, **27**, 64–73.
9 Q. Lei, J. Luo, B. Peng, X. Wang, P. Xiao, P. Wang, L. He, B. Ding and X. Geng, *Pet. Explor. Dev.*, 2019, **46**, 937–942.
10 E. Jafarbeigi, E. Kamari, F. Salimi and A. Mohammadidoust, *J. Pet. Sci. Eng.*, 2020, **195**, 12.
11 P. Liu, H. Yu, L. Niu, D. Ni, Q. Zhao, X. Li and Z. Zhang, *Chem. Eng. Sci.*, 2020, **228**, 11.
12 M. Jalilian, A. Tabzar, V. Ghasemi, O. Mohammadzadeh, P. Pourafshary, N. Rezaei and S. Zendehboudi, *Fuel*, 2019, **251**, 754–762.
13 W. Tian, K. Wu, Y. Gao, Z. Chen, Y. Gao and J. Li, *Energy Fuels*, 2021, **35**, 5643–5670.
14 J. Gong and W. R. Rossen, *Fuel*, 2018, **223**, 470–485.
15 C. Wang, H. Gao, Y. Gao and H. Fan, *Energy Fuels*, 2020, **34**, 9275–9282.
16 Z. Yang, X. Liu, H. Li, Q. Lei and X. Wang, *Pet. Explor. Dev.*, 2019, **46**, 739–745.
17 L. Yang, H. Wang, Z. Zou, Q. Jiang, J. Zhang, J. Xu and J. Cai, *Energy Fuels*, 2021, **35**, 15995–16006.
18 H. Umeobi, Q. Li, L. Xu, Y. Tan, L. Xu, Y. Zhong and C. C. Onyekwena, *Energy Fuels*, 2021, **35**, 15856–15866.
19 B. Hou, F. Zhang, S. Wang, H. Fan, D. Wen, S. Gao, Y. Tian, X. Yang, H. He and X. Zhang, *Energy Fuels*, 2022, **36**, 1316–1325.
20 Y. Ding, X. Yu, X. Liu, L. Liang and J. Xiong, *Energy Fuels*, 2021, **35**, 18518–18532.
21 D. C. Standnes, L. A. D. Nogaret, C. Hung-lung and T. Austad, *Energy Fuels*, 2002, **16**, 1557–1564.

22 A. Habibi, Y. Esparza, Y. Boluk and H. Dehghanpour, *Energy Fuels*, 2020, **34**, 12301–12313.
23 J. Zhang, L. Tian and H. Zhang, *Oilfield Chem.*, 2021, **38**, 184–190.
24 A. Karimi, Z. Fakhroueian, A. Bahramian, N. Pour Khiabani, J. B. Darabad, R. Azin and S. Arya, *Energy Fuels*, 2012, **26**, 1028–1036.
25 J. Giraldo, P. Benjumea, S. Lopera, F. B. Cortés and M. A. Ruiz, *Energy Fuels*, 2013, **27**, 3659–3665.
26 L. Hendraningrat and O. Torsæter, *Energy Fuels*, 2014, **28**, 6228–6241.
27 S. Lim, H. Horiuchi, A. D. Nikolov and D. Wasan, *Langmuir*, 2015, **31**, 5827–5835.
28 S. Al-Anssari, A. Barifcani, S. Wang, L. Maxim and S. Iglauer, *J. Colloid Interface Sci.*, 2016, **461**, 435–442.
29 C. Dai, X. Wang, Y. Li, W. Lv, C. Zou, M. Gao and M. Zhao, *Energy Fuels*, 2017, **31**, 2663–2668.
30 R. N. Moghaddam, A. Bahramian, Z. Fakhroueian, A. Karimi and S. Arya, *Energy Fuels*, 2015, **29**, 2111–2119.
31 J. Zhang, Q. Di, S. Hua, F. Ye, Y. Li and W. Wang, *Pet. Explor. Dev.*, 2018, **45**, 910–917.
32 D. T. Wasan and A. D. Nikolov, *Nature*, 2003, **423**, 156–159.
33 A. Nikolov, K. Kondiparty and D. Wasan, *Langmuir*, 2010, **26**, 7665–7670.
34 K. Kondiparty, A. D. Nikolov, S. Wu and D. T. Wasan, *Langmuir*, 2011, **27**, 3324–3335.
35 H. Zhang, T. S. Ramakrishnan and A. Nikolov, *J. Colloid Interface Sci.*, 2017, **511**, 48–56.